20th Annual Conference of the Canadian Nuclear Society
Montreal, Quebec, Canada / May 30 - June 2, 1999

DETERMINING PROMPT FRACTIONS OF IN-CORE FLUX DETECTORS DURING FULL-POWER OPERATION IN CANDU

by
B. Sur, P. Kumli, J.P. Johnston, and P.D. Tonner
Atomic Energy of Canada Ltd., Chalk River, Ontario K0J 1J0
1999 April

ABSTRACT

This paper presents analysis of in-core flux detector (ICFD) response data acquired during reactor full-power operation in Darlington unit 1 and in Point Lepreau. The purpose of the analysis is to determine the high-frequency response or "prompt-fraction" of the reactor control and safety system ICFDs. Two types of ICFD response data are analyzed: (a) high-fidelity (16-bit), high-speed (100 Hz, 50 Hz) data acquired during near 100% full-power, steady-state reactor operation, and (b) 16-bit, 6 s sampling interval data acquired during a rapid power reduction of approximately 2% just prior to refueling (in Point Lepreau only). Under the assumption of a constant in-core flux-shape during near steady-state operation, it is shown that the high-frequency ICFD gain can be determined to a statistical accuracy of the order of a percent, comparable to the accuracy of effective prompt fractions determined from reactor trip tests. Systematic inaccuracies, due to the analysis assumptions, are explored. Other reactor-core and control-system characteristics that can be ascertained from high-fidelity, high-speed in-core flux detector response data are briefly discussed.

The results demonstrate that high-fidelity, high-speed ICFD response data acquired during normal station operations can serve as an on-line health monitoring or surveillance tool for CANDU reactor-core instrumentation, control and safety systems. In particular, ICFD prompt fractions, an important parameter of control and safety system performance, can be determined to an accuracy comparable to the accuracy from reactor trip tests. These data provide timely information about performance and can aid in planning for maintenance work during outages. The paper makes recommendations for the routine acquisition and use of such data in operating CANDU stations.

1. INTRODUCTION

1.1. Background and Motivation

In-Core Flux Detectors (ICFDs) are critical components in CANDU safety and control systems. The response time of an ICFD to a change in local flux or power depends on its dynamic response characteristics, particularly its prompt response or prompt fraction. The ICFD dynamic response parameters (prompt fraction and amplitudes of lag terms) change due to burn-up of the ICFD constituent materials as the ICFD ages. Thus the dynamic response of aging ICFDs have to be periodically monitored to ensure that they can still provide an adequate control and safety margin.

In the past, all domestic CANDU stations have periodically undertaken manual reactor trip tests to verify that the installed ICFDs satisfy minimum prompt fraction requirements. Reactor trip tests, however, are infrequent, expensive and somewhat stressful to station hardware. Therefore, it is desirable to investigate whether ICFD responses during reactor full-power operations can be analyzed to extract their dynamic response, in particular their prompt fraction. The ICFD response during two modes of full-power operation are considered, steady state and small power maneuver. In the first mode the ICFD responds to fluctuations in the local flux (typically one percent peak-to-peak) brought about by the restoring action of the reactor control system to reactivity perturbations caused by small vibrations and by fluctuations in temperature, flow and other sources of "process noise". In the second mode, the ICFD responds to small induced perturbations in the global reactor flux, for instance when a rapid manual power reduction (typically a few percent) is undertaken just prior to on-power refueling.

Data and prompt fraction analysis results from both types of ICFD responses, measured during normal reactor full-power operation at Darlington Nuclear Generating Station (DNGS) unit 1 and at Point Lepreau Generating Station (PLGS), are presented and discussed in this paper.

1.2. Summary of Prompt Fraction Analysis Methodology

Data acquired during reactor steady-state, near 100% operation at DNGS and PLGS were analyzed by fast Fourier transform (FFT) based techniques. All ICFD signals were observed to undergo highly coherent oscillations, with about 1% peak-to-peak amplitude, at a particular frequency for each reactor - approximately 0.25 Hz for DNGS unit 1, and 0.16 Hz for PLGS. It was *assumed* that the spatial flux shape remains constant during the flux oscillation at this coherent frequency, i.e., the fractional change in flux (as a function of time, at this particular frequency) was the same throughout the reactor. Under this assumption, the ratio of any normalized ICFD signal (in the frequency domain) to a normalized reference signal, at this coherent frequency, yields the transfer function between the two signals. The magnitude of the transfer function (gain) at the relatively high frequency of maximum coherence (0.25 Hz and 0.16 Hz in DNGS and PLGS respectively) was identified as the prompt fraction of the ICFD signal relative to the reference signal. This relative value was normalized (scaled) to the absolute prompt fraction of the reference signal to obtain the absolute prompt fraction of the ICFD. The statistical uncertainty in the high-frequency gain or prompt fraction obtained by the above procedure was assessed from the coherence between the ICFD signal and the reference signal. The normalized high-frequency gains were compared to the Effective Prompt fractions (EPfs) of the same ICFDs, obtained in a trip test following the steady-state data acquisition. This comparison allowed an assessment of whether the steady-state high-frequency gain values were limited by systematic errors due to the assumption of constant in-core flux shape, or whether there was room for improvement via better statistical accuracy.

Data for the ICFD responses during a rapid, 2% power reduction was available only at 6 s intervals from PLGS. Visual examination of the data from all ICFDs and external ion chambers (ICs) showed that the flux shape in the reactor remained approximately constant during this power reduction. A reference 100% prompt dynamic flux signal was constructed by averaging

the signals of all 8 available ICs. Individual ICFD signals were fitted in the time-domain, via least squares minimization, to this reference signal, with the ICFD prompt fraction as one of the fitting parameters. Results for the ICFD prompt fractions obtained by this methodology were also compared to the EPfs obtained in the immediately following reactor trip test, to assess the uncertainties.

The statistical error for each of the two methodologies for obtaining ICFD prompt fractions during normal full-power reactor operation, described above, can be improved by repeating the data acquisition or obtaining longer time sequences of data. However, the actual accuracy of the prompt fraction determination will be limited by the systematic error in the analysis assumption - that the flux shape remains constant throughout the reactor-core during the steady-state flux oscillations or power reduction. Although longer time sequences of data are not available at this time, this work indicates that there is room for improvement in the statistical accuracy before the systematic error limit is reached - possibly at around 1% accuracy, comparable to the accuracy of EPf measurements from run-down tests.

2. DATA

Data from DNGS and from PLGS were used for this analysis.

2.1. DNGS Data - Reactor Near 100% FP Steady-State Operation

The DNGS data was acquired in 1997 April by the AECL noise analysis system (NAS). The NAS input for each acquisition channel was connected directly to the output of the ICFD current-to-voltage amplifier via an optically isolated, unity gain amplifier, and contained an adjustable, multi-pole, anti-aliasing filter. The filtered signals were multiplexed into a 16-bit analog-to-digital converter (ADC). The data used in this analysis was acquired at 100 Hz (i.e. 10 ms intervals), for about 2 hours, during reactor full-power steady state operation just prior to a power reduction to 60% full power (FP), followed by a manual SDS2 (poison injection) trip test.

Data from 13 vertical inconel ICFDs in safety-system channel F, 12 horizontal platinum-clad inconel ICFDs in safety-system channel J, and the linear ion-chambers (ICs) in channels F and J were acquired by the NAS, and used in the analysis. DC-offsets (approximately millivolts) due to the unity gain isolation amplifiers in each acquisition channel were measured and subtracted from the data, as were the 0.5 volt station dc-offset applied to all neutronics signals. There did not appear to be any problems associated with data drop-outs, or any other type of data “glitches” in the NAS-acquired data.

Figure 1 a) shows time-sequence data and figure 1 b) shows a histogram of the signal amplitudes for a typical signal (ICFD 1F). The measured signal has been normalized (divided) by the average signal value over the entire time span. The signal oscillates around a value of 1, with a peak-to-peak variation of approximately 1%. Figure 2 a) shows the time-sequence data and figure 2 b) shows the amplitude distribution histogram of the normalized signal from another detector (ICFD 12F). The peak-to-peak variation in this signal is significantly larger than in the typical signals, thus the signal can be considered to be “noisy”.

2.2. PLGS Data - Reactor Near 100% FP Steady-State Operation

The PLGS data was acquired in 1997 November by the PLGS High Speed Data Logger (HSDL). The HSDL is a continuously operating, 16-bit, 50 Hz (i.e. 20 ms interval) data acquisition system that collects data from almost all neutronic devices (safety and control ICFDs, ICs, reactivity control devices) into a first-in-first-out (FIFO) data-buffer. During normal steady-state operation, simultaneously acquired data are recorded only once every 6 s. However, when triggered by a reactor transient such as a trip, the FIFO buffer is dumped, yielding about 5 minutes of high-speed data immediately preceding the trigger event, followed by high-speed data collection for a further 5 minutes. To acquire the approximately 1 h of steady-state data analyzed in this report, the HSDL was manually triggered to continuously dump its high-speed data buffer. Subsequent to this steady-state data acquisition, the reactor power was reduced to 77% FP, and then the reactor was manually tripped via SDS1 (rod-drop). High-speed detector response data to the manual trip were also available.

Data from all platinum-clad inconel ICFDs (RRS and SDS) and from all ICs in the PLGS core were available. Reactivity control device positions were also available, in particular the liquid-zone controller (LZC) levels from all 14 zones. There is no specific anti-aliasing filtering in the HSDL. However, the isolation amplifiers which precede the HSDL ADCs for RRS channel A, and for SDS channels D, E, F, G, H, and J, have an approximate first order time-constant of 50 ms (i.e. a 3 dB roll-off of approximately 3 Hz) which provides protection against aliasing (since the Nyquist cut-off frequency for the HSDL is 25 Hz). RRS Channel C has higher band-pass, 1 ms response time isolation amplifiers, which do not provide adequate protection from aliasing.

The HSDL inputs for the safety system ICFDs (i.e., channels D, E, F, G, H, J) were taken from the buffered outputs of the trip test alarm (TTA) modules following the dynamic signal compensators (DSCs) in the ICFD electronics loop. Thus the safety system ICFD signals, as measured by the HSDL, are characterized by the combined dynamic response, including prompt fraction, of the ICFD and the DSC. The design prompt fraction of the DSC is 1.066, i.e., its effect is to increase the ICFD prompt fraction by approximately 6.6%.

There were numerous instances of data drop-outs and spurious signals in the PLGS steady-state data-set. After manual rejection of the most glaring data “glitches”, the analysis routines were tuned to automatically detect, flag and reject blocks of bad data.

Figure 3 a) shows the raw time sequence data and figure 3 b) is a histogram of the signal amplitude for a typical signal from PLGS (ICFD 1D). As in DNGS, there is a peak-to-peak amplitude variation of about 1% in the signal measured during reactor steady-state operation. Figure 4 is an example of a noisy signal (Linear ion-chamber signal from channel H) in the PLGS data-set. Several other signals were found to be atypical or noisy, even after the data “glitches” were discarded.

2.3. PLGS Data - Small Power Derate During Near 100% FP Operation

Following data acquisition during reactor steady-state operation (section 2.2), and before power reduction to 77% FP, PLGS undertook a small power de-rate maneuver where the reactor power was manually reduced by approximately 2% via the reactor regulating system (RRS). The power ramp rate was approximately 1.5% FP per minute. Such small power maneuvers are undertaken regularly in CANDU stations, usually just prior to on-power refueling, in order to avoid a reactor trip from fluctuations in the neutron flux due to the sudden addition of positive reactivity.

Unfortunately, the HSDL was not triggered to dump high-speed data during this maneuver. Neutronics and reactivity device data from the HSDL was available at 6 s intervals only. The 6 s interval data were extracted into ASCII files and imported into Microsoft EXCEL for time-domain analysis.

Approximately 1 hour (3000 s) of data were extracted for analysis. There were no obvious instances of data "glitches" in this stretch of data.

3. ANALYSIS METHODOLOGY FOR REACTOR STEADY-STATE DATA

In general, the data-analysis for the reactor steady-state data were performed using fast Fourier transform (FFT) techniques. The Fourier analysis was performed in MATLAB, using the following functions available in the Signal Processing Toolbox [1]:

fft: Computes the complex, discrete fast Fourier transform (FFT) over the full Nyquist range. For a long data series, the Fourier transform is performed sequentially for specified lengths of data (block-size) and added. There is provision for data-windowing (to reduce side-lobes in the power spectrum), data de-trending (to improve numerical accuracy and remove low frequency lobes), and partial overlapping of successive blocks (to make full use of the signal statistics).

psd: Computes the one-sided power spectral density (PSD) - the squared magnitude of the FFT for positive frequencies only. It provides an estimate of the power (square of signal amplitude) in each frequency bin of the discrete FFT.

csd: Computes the cross-power spectral density (CPSD) of two signals. The CPSD is the product of the conjugate FFT of one signal and the FFT of the other. It is also the FFT of the time-domain correlation function or lag between the two signals.

cohere: Computes the coherence or normalized one-sided cross-power spectral density (squared) between two signals. The coherence between two signals, X and Y is calculated as $|CPSD(X,Y)|^2/\{PSD(X)\cdot PSD(Y)\}$. It is a statistical measure of the covariance, i.e., of the uncorrelated noise between two signals, and is only valid for analysis of multiple blocks of data. Its value ranges between 0 and 1. A value of 1 or 100% in any frequency bin

implies that the two signals are perfectly correlated at that frequency, i.e. there is no un-correlated noise power in that frequency bin.

tfe: Computes the complex transfer function in the frequency domain (positive frequencies only) between any two time-domain signals. The transfer function is the ratio of the FFTs of the two signals. As in the **fft**, **psd**, **csd** and **cohere** functions, a long time sequence of data can be broken up into blocks, and the transfer function computed as the average over all the blocks with provision for windowing, de-trending and partial block overlap. The tfe algorithm calculates the transfer function of signal Y with respect to a reference signal X as CPSD(X,Y)/PSD(X).

angle: This function provides the argument or phase angle for a complex number. If two signals have a coherence near unity at a particular frequency, then the phase angle of the complex ratio of their FFT values at that frequency (i.e., the transfer function value) indicates the phase or equivalently the time lag between them.

For the Fourier analysis, all data were converted to MATLAB binary format and stored in separate files for each ICFD. MATLAB routines were written to automatically load, analyze and plot various combinations of signals. All signals were assumed to have arbitrary calibration factors. Since we are only interested in the fractional changes in the signals, each signal data-point was normalized (i.e. divided) by the average value of the entire data-series. Thus each signal oscillated about a value of 1. After some experimentation, the data was Fourier analyzed using mean de-trending, Hanning windowing, and an overlap of half the block-size. This is fairly standard procedure in noise analysis.

A block size of 8192 was chosen for the DNGS data to yield a frequency bin-width of 0.0122 Hz (100 Hz sampling rate / 8192 bins). With overlap, the analyzed data for DNGS contained 200 blocks. Similarly, a block size of 4096 was chosen for the PLGS data to yield a frequency bin-width of 0.0122 Hz (50 Hz sampling rate / 4096 bins). With overlap, the PLGS data contained 100 blocks. The above block sizes appear to yield a near optimum frequency bin-width. Larger bin widths (i.e., smaller block-size, more blocks in the given time sequence data) appear to contaminate the signal at the point of interest - 0.25 Hz for DNGS and 0.16 Hz for PLGS with in-coherent data from adjacent frequency intervals. Smaller bin-widths do not appear to provide any advantage in increased coherence at the point of interest, while leading to less statistical accuracy due to a smaller number of blocks in the acquired time sequenced data.

The **psd** and **tfe** functions (i.e. **.m** files) in MATLAB were modified so that the data could be checked for outliers. Any block of data with an outlier data point was rejected and not used in the block-averaging procedure. To compute the high-frequency gain, the **tfe** and **cohere** functions were computed between individual ICFD signals and a reference signal. The MATLAB routine then searched for the frequency bin with the largest coherence. The magnitude of the tfe function in this bin is the high frequency gain quoted in this paper.

3.1. Reference Signals

The ICFD prompt fraction is identified as the high frequency gain of the ICFD signal. The gain at any frequency is the absolute value of the transfer function at that frequency. The transfer function has to be measured relative to another signal, preferably one with a known 100% prompt response or unity gain independent of frequency. This is the reference signal. The transfer function is meaningful only at frequencies where the coherence is high, i.e. there is high confidence that the reference signal and the ICFD signal are sampling the same underlying flux perturbations.

It was initially thought that the 100% prompt reference signal could be obtained from the linear ion-chamber signals. During the analysis it was found that, particularly in the case of DNGS, the coherence between the ex-core IC and the ICFDs was significantly lower than that between any two ICFDs. Evidently, for a core as large as DNGS, the flux perturbations sampled by the ex-core IC and the in-core ICFDs are significantly different. Furthermore, in order to reduce the spatially and temporally un-correlated noise in the reference signal, it is desirable to average signals from several different locations in the reactor core. This was not possible for ICs in the case of DNGS because data from only one "good" IC - the channel J IC - was acquired. Data glitches prevented averaging the channel G, H and J IC signals in PLGS.

Therefore, the individual ICFD transfer functions were evaluated against a number of different reference signals, obtained by averaging the data from groups of ICFD signals. The high-frequency gain obtained for individual ICFDs in this case is a relative value, and must be scaled (or normalized or multiplied) by the gain of the group averaged reference signal.

The transfer function methodology would be tremendously improved if there were one or more 100% prompt reference detectors inside the core, particularly in the case of a large core such as DNGS. Such a prompt in-core reference signal could be obtained from a miniature fission chamber or a Cobalt-emitter ICFD.

3.2. Statistical Accuracy of the Frequency-Domain Gain

The following expression was used to estimate the 1-σ statistical error, $\sigma(|\text{tfe(f)}|)$, in the high-frequency gain estimate, $|\text{tfe(f)}|$ at frequency f, for the steady-state signal analysis.

$$\frac{\sigma(|\text{tfe(f)}|)}{|\text{tfe(f)}|} = \sqrt{\frac{1}{n}\cdot\left(1-\sqrt{\text{Coh(f)}}\right)} \qquad (1)$$

Coh(f) is the value of the coherence function between the ICFD signal and the reference signal at frequency f, and n is the number of independent data blocks - 200 for DNGS and 100 for PLGS. The expression is true only for signals whose relative phase is statistically distributed around zero. The uncorrelated noise is assumed to be "white" noise.

4. RESULTS OF REACTOR STEADY-STATE DATA ANALYSIS

4.1. General Observations

Figures 1 and 3 show results of the Fourier analysis for "typical" ICFD signals from DNGS and PLGS respectively. Figures 1 c) and 3 c) are PSD plots, showing the full Nyquist range on a log-log scale in the lower frame, and the region below 1 Hz on a linear scale in the upper frame. Figures 1 d) and 3 d) show the transfer function magnitude (in dB), phase and coherence between the typical DNGS ICFD signal and a core-averaged reference signal. The particular reference signals used for these figures are the average of all channel F ICFDs for DNGS (figure 1 d)) and the average of all ICFDs in channels D, E, and F for PLGS (figure 3 d)). Other core-averaged reference signals yield similar results.

Figures 2 and 4 are similar to figures 1 and 3 respectively, but show the results for atypical or noisy signals for each reactor.

The PSDs in figures 1 and 3 show well-resolved structure over the full Nyquist range. This demonstrates the adequacy of ~100 blocks of data taken with 16-bit data acquisition systems (such as the AECL NAS and the PLGS HSDL) for noise analysis of in-core instrumentation in CANDU, without the need for hardware dc-subtraction.

Aside from possible noise pick-up in the electronics, the structure in the detector PSD plots reflects the time structure of local flux oscillations, convoluted by the detector response function. There can be two general sources for such flux oscillations: (1) reactivity disturbances in the reactor-core caused by temperature, pressure or flow fluctuations in moderator, coolant or fuel, and (2) very local disturbances in the flux seen by the detector due to relative movement of local core components, i.e. vibrations of the flux-detector tubes or of nearby fuel channels or bundles. The first type of disturbance (reactivity fluctuations) will affect all detectors via the closed-loop transfer function between reactivity and flux of the reactor and control system. Indeed the shape of the PSDs for frequencies below 1 Hz is consistent with the expected closed-loop transfer function for a controlled reactor[2] The peak in the PSDs (hence in the reactor transfer function) at about 0.2 Hz is due to a combination of the natural frequency of the control system, and of reactor-kinetics parameters, mainly the neutron generation-time, delayed neutrons and the reactivity power coefficient. The sharp peaks at frequencies greater than 0.5 Hz are presumably caused by either electrical pick-up in individual detector-electronics loops or by local flux variations; i.e. core component vibrations.

The coherence plots (figures 1 d) and 3 d)) reinforce the above interpretation. The coherence between all detectors is generally larger below 1Hz, and drops to negligible values above this frequency. This indicates global, correlated flux oscillations due to reactivity fluctuations below 1 Hz. Coherence plots of selected pairs of detectors show sharp peaks above 0.5 Hz, indicating a common source of vibration at that natural frequency. Such detectors are generally located in the same flux detector assembly or along the same fuel channels.

Inter-comparison of the signal amplitude distributions (histograms), PSDs and coherence plots can reveal atypical (noisy, quiet or un-correlated) detector signals which may be indicative of malfunctioning detectors, malfunctioning electronic loops or poor spatial flux control. For example, in DNGS, the PSD of ICFD 12F (figure 2 c)) shows a high base-line noise power, and a poorly resolved 0.25 Hz peak. The presence of unusually large uncorrelated noise is also indicated by the low peak value of the coherence (figure 2 d)) at the resonant 0.25 Hz frequency. Similar observations can be made about the PLGS channel H Linear IC signal (figure 4 c) and 4 d)). The present study uncovered several detector signals with such "atypical" steady-state PSD and coherence "signatures" in DNGS and PLGS.

If signals are available at two or more points around the reactor-control system loop, then the effects of the unknown reactivity disturbance input can, in principle, be eliminated and the reactor-control system closed loop parameters can be measured (by a parametric fit of the transfer function) for reactor-core surveillance and safety assessment purposes. The measurable parameters include the reactivity worth of the zone controllers, controller time-constants, the neutron generation time, the reactivity power coefficient, etc. [3],[4]. It should be possible to do this, for instance, for the PLGS data, where data is available at two points in the loop: reactor flux and LZC levels. The transfer function between the LZC level signals and the RRS detectors exhibit high coherence up to a frequency of approximately 1 Hz, indicating that the transfer function between these signals can be measured with accuracy. An additional useful signal pick-off point for surveillance of the control system instrumentation would be the valve-lift signal from the controller.

4.2. ICFD Prompt Fraction Estimation

Coherence plots between detector signals (figures 1 d) and 3 d)) show a broad maximum near 1, coinciding in frequency with one of the peaks in the PSD spectrum of the corresponding detectors. This occurs at a value near 0.25 Hz in DNGS and 0.16 Hz in PLGS. The phase between any pair of analyzed detector signals is seen to be near zero at the frequencies corresponding to this coherence maximum and PSD peak. The DNGS PSD plots also show peaks near 0.16 Hz and 0.22 Hz, which are less coherent than the 0.25 Hz peak. The origin of these extra peaks is not known. In general, the differences in the low-frequency PSD structure between DNGS and PLGS detectors show that there are fundamental differences between the reactor kinetics and control system parameters of these two reactors.

It was *hypothesized* that the coherence peak near 1 between all detectors corresponds to global oscillations of the fundamental flux shape in the reactor. The implicit *assumption* was that the controlled-reactor *spatial* transfer function at this particular *temporal* frequency is flat. If this is the case, then the amplitude of the correlated part of the fractional change in flux, $\delta\phi/\phi_0$ would be equal at all detector locations at this frequency. This frequency (0.25 Hz in DNGS, 0.16 Hz in PLGS) is well above the break frequency corresponding to the smallest time constant in the ICFD transfer function (3.9 s), so the amplitude of the ICFD normalized response (as is analyzed in this work) is expected to be simply $Pf \times (\delta\phi/\phi_0)$; where Pf is the ICFD prompt fraction. If these conditions are true, then the magnitude of the transfer function between the normalized response

of any two detectors will be the ratio of their prompt fractions. In particular if one of the comparison detectors is chosen to have a standard prompt fraction (e.g. the ion chambers, with Pf = 1), then the prompt fraction of all other detectors can be obtained. Unfortunately, the coherence (i.e. signal to statistical noise ratio) between the ICFD signals and the ex-core ICs is not good, particularly in the case of DNGS unit 1. This necessitates the use of averaged ICFD signals as the reference flux signal. Averaging (at each point in time) statistically removes un-correlated spatial flux fluctuations, hence yields a better flux reference signal than a single ICFD signal. The high-frequency gain of individual detectors with respect to these averaged signals must be re-normalized to either the design value or the trip EPf of the group averaged ICFDs.

Even at the maximum, the coherence is not 1, implying that there is an un-correlated noise contribution to the ICFD signal. The effect of the un-correlated amplitude fluctuations in the frequency spectrum of the signals is reduced by the block averaging scheme employed by the MATLAB **tfe** routine.

Table 1 shows the transfer function parameters (gain, phase, coherence) at the frequency of maximum coherence for all DNGS measured signals vs. the average signal of all channel F ICFDs (one of several reference signals used in the full analysis). While the coherence between in-core signals was generally 90% or more, that between the ion-chambers and the reference signals was notably lower. This indicated that the ion chambers were not a good source of reference flux for the analysis. The coherence between the average channel J signal and the average channel F signal (last row of Table 1) was very good, and the gain was almost exactly equal to the ratio of the design value prompt fractions for these detector types (channel F has Inconel ICFDs with design Pf = 1.05; channel J has Pt-clad Inconel ICFDs with design Pf = 0.9).

To compare the high-frequency gain values to prompt fractions for individual detectors, the gains had to be normalized to the gain (or Pf) of the reference signals. The normalization was done as follows: given the good agreement of the channel J average - channel F average gain to the design value, the gains of all individual signals were scaled by a common multiplicative factor such that the normalized gain of the average channel J signal becomes 89.9% - the design value prompt fraction for Pt-clad Inconel ICFDs.

The normalized gains and its estimated statistical uncertainty are given in Table 1 and compared to Effective prompt fraction values derived from the immediately following trip test. Standard deviations of the gains of ICFDs grouped by channel were also tallied and compared to those from the trip. The statistical and systematic uncertainties in individual ICFD EPfs derived from trip tests has been estimated elsewhere to be about 2%. However, in practice it is found that trip EPfs are reproducible at the 0.1% to 0.2% level for individual ICFDs from one trip to another. The channel population average gains agree well with the channel average trip EPfs. The channel population standard deviation of the gains, derived from the steady-state data, is about a factor of 2.5 larger than that derived from the trip (4.5% to 6% as opposed to 1.7% to 2.7% for various groups of signals). It is not clear whether this higher population standard deviation. is the result of the larger statistical uncertainty in the steady-state data analysis, or whether it represents the inherent limit of this methodology due to violation of the assumption of constant spatial flux shape. If the latter is the case, then this number (the population standard deviation) indicates how

well the control system maintains the spatial flux shape in the reactor during steady-state operation.

The Linear IC gain values obtained from the steady-state analysis are clearly inconsistent with the expected 100% prompt response. One of the ICFDs, the Linear channel F signal was known to be malfunctioning, as also indicated by the trip EPf value. The exact cause of the low gain value for the Linear J signal is not known. Two ICFD gain values, those of ICFDs 12F and 1J, can clearly be considered to be outliers in the distribution of measured values. The cause is not known, except to note that both these ICFDs are located in the outer periphery of the core. ICFD 12 F was also noted to have an atypical noise signature (figure 2).

Figure 5 a) illustrates the correlation between the normalized high frequency gains measured via steady-state analysis and the EPfs for the same ICFDs measured in the SDS2 trip test immediately following the steady-state data acquisition. As noted earlier, the channel average prompt fractions agree well between the two methods, but there is a larger spread in individual values in the case of the steady-state gains. Nevertheless, it appears to the eye that a correlation does exist, and that an improvement in the statistical accuracy of the steady-state gains will lead to a better correlation (smaller spread).

Table 2 shows the transfer function parameters (gain, phase and coherence) for the frequency of maximum coherence for selected PLGS signals versus the average signal from all ICFDs in channels D, E, and F, used as the reference signal. For brevity, individual ICFD results are shown only for channels D (SDS1) and J (SDS2). The values for averaged signals for all detectors in the other channels are shown. No normalization was required to translate the gain values to prompt fractions. This is because the channel D, E, F ICFD signals are already dynamically compensated to 99.5% average prompt response (as seen from the trip EPfs, as well as from earlier studies). Thus a direct comparison of the gain at 0.16 Hz and the trip EPfs is presented in Table 2.

As in the case of DNGS, the external linear IC signals did not exhibit as high a coherence with the in-core ICFD signals, as did the in-core signals themselves. This was reflected in the larger spread in gain values, and the higher statistical uncertainty in individual values of the linear IC gains vs. the reference signal. The channel G, H and J linear ion chambers had atypical gain values, low coherence and also exhibited atypical amplitude distributions and PSDs. These are indications of improper functioning or improper data acquisition connections for these signals.

The RRS ICFDs (channels A and C) showed a larger high-frequency gain (~100%) than expected (~90%). Evidently there was a larger amplitude of the 0.16 Hz flux oscillations at the location of these ICFDs compared to the average core. This is not surprising since these ICFDs are located adjacent to the LZC absorbing water compartments and experience the additional effect of the coherent, oscillating flux depression due to the water level in these compartments. The local flux depression effect is well known for the case of control rods [2]. The effect of this “LZC shadow factor” is further discussed in section 5, where it is also shown that the average effect is ~ 10%.

For SDS ICFDs (channels D, E, F, G, H, J), the channel average signal gains, and also the population averages of the individual detector gains in each channel show good agreement with

trip EPf values (Table 2). The spread in the individual gains (channel population 1-σ values) is a factor of 2 to 4 higher than the spread in trip EPfs. The correlation between the steady-state gains and trip EPfs for individual SDS ICFDs is illustrated in figure 5 b). The same arguments apply to these spreads as were applied in the case of the DNGS analysis above.

5. ANALYSIS METHODOLOGY FOR SMALL POWER DERATE DATA

The small power de-rate data from PLGS was analyzed for ICFD prompt fractions using least-squares fitting in the time domain. It was assumed that a prompt flux reference signal, $\phi(t)$, would be available for each ICFD. Details of the reference flux used are given in section 6. The ICFD response to flux is assumed to be the sum of a prompt response (prompt fraction) and a number of first order lag terms with amplitudes, a_i and time constants τ_i. In the Laplace (complex frequency) domain, the normalized response of the detector, $R(s)$, can be written in terms of the normalized reference flux, $\phi(s)$ as:

$$R(s) = \phi(s)\left[Pf + \sum_i \frac{a_i}{(1 + s\tau_i)} \right] \qquad (2)$$

where the prompt fraction, Pf, is defined as:

$$Pf = \left(1 - \sum_i a_i \right) \qquad (3)$$

5.1. Time-Domain Analysis Algorithm

In the time domain, the normalized detector response at time t_2, $R(t_2)$, can be written in terms of the normalized reference flux and the response at an earlier time, t_1, as:

$$R(t_2) = \phi(t_2)\left(1 - \sum_i a_i \right) + \sum_i a_i R_i(t_2) \qquad (4)$$

where each lag term, $R_i(t)$, is given by:

$$R_i(t_2) = R_i(t_1) e^{-\frac{t_2 - t_1}{\tau_i}} + \frac{1}{\tau_i} \int_{t_1}^{t_2} \phi(t)\, e^{-\frac{t_2 - t}{\tau_i}}\, dt \qquad (5)$$

Equations (4) and (5) define a recursive procedure (an Infinite Impulse Response or IIR digital filter) for calculating the expected detector response as a function of time when the input or reference flux is known. At every instance of time, the value of the individual lag terms and the new value of detector response can be calculated from the reference flux and the previous values of the lag terms. In the present case, the reference flux and the detector response are measured at

time intervals of 6 s. In other words, $(t_2 - t_1) = \Delta t = 6$ s. One needs a model of $\phi(t)$ between the discrete measurements in order to evaluate the integral in equation (5). A simple model is to assume that $\phi(t)$ between t_1 and t_2 is the average of $\phi(t_1)$ and $\phi(t_2)$, i.e., $\phi(t) = (\phi(t_1) + \phi(t_2))/2$ for $t_1 < t < t_2$. With this assumption, equation (5) can be evaluated as:

$$R_i(t_2) = R_i(t_1)e^{-\frac{\Delta t}{\tau_i}} + \frac{\left[\phi(t_2) + \phi(t_1)\right]}{2}\left\{1 - e^{-\frac{\Delta t}{\tau_i}}\right\} \qquad (6)$$

The recursive filter defined by equations (4) and (6) was implemented via cell formulas in Microsoft Excel, such that given a column of data containing ϕ, the spreadsheet produced an adjacent column containing the detector response, R. Parameters which could be adjusted via cells included two lag term amplitudes and time constants, their initial values, $R_i(0)$, and a dc-offset term (equivalent to a lag-term amplitude with ∞ time-constant). The prompt fraction was calculated in another cell from equation (3). Measured detector responses were copied into the worksheet as a column of data, and the sum of squared differences between the measured and calculated response was tallied in a cell. The value of this cell was minimized using the SOLVER function, via optimization of the parameter cell values. Macros automated data transfer, least squares minimization and generation of tables of optimized parameters for the entire set of detectors.

5.2. LZC-Level Shadow Factor

As explained in the results (section 6), the response of detectors adjacent to the liquid zone controllers was found to be influenced (anti-correlated) with the LZC-level signal. It was hypothesized that in addition to the reactor-wide temporal flux variation, these particular detectors experienced the additional effect of flux depression due to the proximity of the neutron-absorbing water in the zone controllers, in other words, they were in the flux "shadow" of the LZCs. To account for this phenomenon, the detector responses were calculated based on an "effective reference flux", ϕ', given by:

$$\phi'(t) = \frac{\phi(t)\left(1-(sf)[L(t)]\right)}{\left(1-(sf)[L(0)]\right)} \qquad (7)$$

where sf was the (adjustable) "LZC shadow factor" parameter, $L(t)$ the fractional zone fill level as a function of time, and the factor in the denominator re-normalized the effective flux to unity at time zero.

6. RESULTS OF SMALL POWER DERATE DATA ANALYSIS

Figure 6 shows normalized, channel-averaged ICFD responses, the average response of all 8 ICs, and the average LZC fractional fill level during and immediately following the small power de-rate maneuver in PLGS. It is clear that all six average SDS channel signals and the average ex-core IC signal track each other closely. The two RRS channel average signals appear to be correlated to

the average IC signals, but, specially in their trend at later times, also appear to be anti-correlated to the LZC fill. As mentioned in section 5.2, this is thought to be due to the flux shadowing effect of the water in the LZCs. The anti-correlation with LZC levels is also evident in a few individual horizontal (SDS2) detectors, located perpendicular but adjacent to a LZC.

Figure 7 shows the normalized signals from all 12 channel D ICFDs. The spread in the normalized signal levels is very small, particularly in the first half of the data. This demonstrates that there was excellent spatial control during the power maneuver. Due to the striking visual correlation of the average ex-core IC signal to individual and channel average ICFD signals, it was decided to use this (the average IC signal) as the reference flux signal. The first 40% of the data, which covers the power maneuver period, was fitted. When the fitting algorithm described in section 5.1 was tried initially, it was discovered that the optimization resulted in only very long time-constants, or only a dc-offset for the lag terms. In retrospect, this is not surprising. Fitting lag term parameters (amplitudes and time-constants) in the time-domain is equivalent to estimating the transfer function parameters at low frequencies in the frequency or Laplace domain. It is known from the steady-state data analysis that there is very little coherence between the detector signals at frequencies significantly lower (or higher) than the 0.16 Hz (= approx. 1/6 s) reactor-wide resonance frequency. In other words, the response of the individual detectors is dominated by un-correlated "noise" or disturbance input at these very low frequencies, and there is no signal left to fit. The detailed ICFD response function can only be extracted if there is a good low-frequency reference signal - this would require a 100% prompt detector located close to the ICFD. Such a reference signal could be obtained by use of the traveling flux detector (TFD) in future data acquisition campaigns. It may also be possible to construct a "good" reference signal by simulating the time-history of the in-core flux distributions, given the measured LZC levels, using a 3D neutron diffusion code such as the Reactor Re-fueling Simulation Program (RFSP).

Although it proved impossible to fit the amplitudes of individual lag terms, i.e., the low-frequency response, it was still possible to calculate the high frequency gain or prompt fraction of individual detectors. The design value of the shortest ICFD lag term time-constant is 3.9 s, corresponding to a corner frequency of approximately 0.04 Hz, well below the coherence peak at 0.16 Hz. Therefore for small flux variations, as was the case, the contribution of the lag terms could be lumped into a single delay amplitude, *a*, with undetermined or very long time-constant, essentially a dc-offset term. The prompt fraction would be (*1-a*). Although a non-linear fitting routine (SOLVER) was used, the fit of the measured flux to the reference flux is essentially a straight line:

$$R(t) = \phi(t) \cdot [1 - a] + a \cdot \langle \phi \rangle, \quad \langle \phi \rangle \cong 1 \qquad \textbf{(8)}$$

Figure 8 illustrates the above concept. The two groups of data points correspond to reactor operation just before and just after the power de-rate maneuver. The magnitude of the power de-rate (i.e. % reduction in power) determines the separation of the two groups of data points, hence the accuracy of the slope (prompt fraction) determination. A reactor trip (near 100% power reduction) is the ultimate power de-rate maneuver.

Table 3 is a compilation of prompt fractions for individual detectors from channel D only (for brevity) and the average values for the results from other channels, as determined by the SOLVER routine. For calculating the values in this table the LZC shadow factor was set to zero for all detectors. Effective prompt fractions (EPf) of individual detectors determined from the trip immediately following this exercise are also listed for comparison.

The channel A and C (RRS channels) ICFD prompt fractions were optimized simultaneously with the shadow factors of the individual LZC levels corresponding to these ICFDs. Table 4 is a compilation of the prompt fractions and LZC shadow factor determined from the fitting procedure.

These results are discussed below.

6.1. Discussion of Prompt Fraction Results from Power De-Rate Data

It is noted that the data acquisition interval of 6 s, without any anti-aliasing filter, was barely adequate for the data analysis. The coherent signal content of the data was centered around 0.16 Hz, close to the Nyquist cut-off frequency for the acquired data. Therefore significant signal aliasing problems were likely present in the data. For a properly filtered signal, or for a signal acquired at somewhat higher sampling frequency, say 1 Hz, it would be possible to significantly improve the signal-to-noise ratio by digital filtering of the data through a pass-band centered around 0.16 Hz.

Table 3 and Table 4 show that channel average ICFD prompt fractions determined from the small power de-rate data agree very well with those determined from trip data. The channel by channel population standard deviations of prompt fraction values from the de-rate data (3% to 7%) is a factor of approximately 3 larger than those determined from trip data (1% to 2%). The agreement between individual LZC shadow factors determined by independent ICFDs in channel A and C is remarkable (Table 4), even though the corresponding channel A and C ICFD prompt fractions show no correlation.

Figure 9 is a scatter plot showing the prompt fractions determined from trip data vs. the prompt fractions from the power de-rate data for all SDS detectors. No correlation was apparent to the eye. It was also verified that there were no obvious correlation between the prompt fraction values and the in-core position of the individual ICFDs. In the absence of any correlations, it was concluded that a large portion of the 3% to 6% standard deviation in ICFDs grouped by channel was due to variations in the spatial flux shape during the power de-rate maneuver. This was a systematic error in the methodology due to the *assumption* of constant flux shape, whose temporal variation was tracked via the average IC reference flux. Alternately, the 3% to 6% channel population standard deviation can be interpreted as an upper limit on spatial variations in flux shape during the maneuver, i.e., a performance indicator for the reactor spatial control system.

Note that the SDS detector signals acquired by the HSDL are downstream of the dynamic signal compensators. The DSCs are designed to be over-prompt by 6%. Therefore this design value of

the DSC over-prompt fraction must be subtracted from the Pfs and EPfs of the SDS detectors in order to estimate their "true" instrumental prompt fractions.

7. CONCLUSIONS

This work shows that high-speed (50 Hz to 100 Hz), high resolution (at least 16-bit) data acquisition systems are sufficient for steady-state signal analysis in CANDU, without the need for hardware dc subtraction. Analysis of the resonance region of the ICFD power spectrum can be achieved by sampling frequencies as low as 2 Hz, if properly filtered against signal aliasing. The analysis of the complete set of steady-state data on neutronics detectors and device positions from PLGS shows the usefulness of such a built-in data acquisition system for monitoring reactor-core components and conditions in CANDU stations during full-power operations. Reactor steady-state data can be obtained without affecting the normal functioning of the station. The results of such surveillance can be used for continuous monitoring of control and safety critical components, especially for aging reactors. Reactor core surveillance can be accomplished prior to shutdowns, and the results can be used in planning and prioritizing maintenance activities during the shutdown. The permanent installation of high speed, high fidelity, on-demand data acquisition systems at all operating and new CANDU stations is recommended.

As touched upon in this note, high-speed data from in-core detectors and reactivity control devices contain a wealth of information, both about reactor-core characteristics and about the detector dynamic response parameters. Fundamentally, the steady-state in-core detector signals depend upon the reactor, control system, and flux detector transfer functions, and may be used to (a) measure and validate these functions during commissioning as well as (b) track changes in these transfer functions as the core ages. The ability to measure fundamental reactor operating parameters (such as LZC valve time-constants, LZC reactivity worth, reactivity power coefficients) during routine reactor operations will provide continuous confidence in the functioning of the reactor, control and safety systems for systems engineers as well as for regulators. A detailed study of the methodology to extract the reactor and control-system parameters from steady-state data in CANDU is recommended.

Systems engineers at CANDU stations often gauge the working condition of reactor components and instrumentation via the historical trend in their measured performance characteristics (e.g. ICFD prompt fractions). The steady-state noise "signatures" of ICFDs, i.e. the measured amplitude histogram, PSD, coherence and transfer function with respect to a standard reference signal, constitute such a performance characteristic. Deviation from either the historical or the typical signature is an indication of ICFD or ICFD electronics loop malfunction. This work has demonstrated the use of such signatures as an early warning indicator of atypical or malfunctioning ICFDs or electronics loops. A historical data-base of steady-state noise signatures from all flux-detectors, for surveillance and historical tracking purposes, is recommended for all operating and new CANDU stations.

The data analyses show that channel average values of ICFD prompt fractions determined from either reactor steady-state or from small power de-rate maneuvers agree very well with those

determined from reactor trip tests. The rms spread (channel population standard deviation) of prompt fraction values determined by the reactor near full-power methods are a factor of 2 to 3 larger than values determined from trip data. The statistical accuracy of individual ICFD prompt fractions, determined from about 1 h of high-speed steady-state data, is also about a factor of 2 larger than trip values. It appears likely that agreement between the reactor full-power methods and the reactor trip methods will improve with larger or repeat steady-state data-sets, i.e., the accuracy of the reactor steady-state method appears to be limited (for approximately 1 hour of data) by statistics and not by systematic inaccuracies. It is recommended that larger data-sets be analyzed, using the methodology developed in this work, to resolve the issue of the ultimate accuracy of the steady-state methodology in CANDU. The benefit to the CANDU nuclear industry lies in the ability to continuously measure and demonstrate compliance with ICFD prompt fraction criteria for safety and control system availability without having to undergo a relatively expensive and stressful reactor trip test.

8. ACKNOWLEDGEMENTS

We would like to thank AECL and OH staff for the use of data acquired by the AECL Noise Analysis System at DNGS unit 1. We also gratefully acknowledge the work of PLGS staff for providing steady-state and small power de-rate data for this project.

9. REFERENCES

1. MATLAB Signal Processing Toolbox User's Guide Version 4, The Mathworks Inc., 1996 December.
2. M.A. Schultz, "Control of Nuclear Reactors and Power Plants", McGraw-Hill Book Co., Inc., (1955).
3. H.W. Hinds, "AECL-KAERI Tandem Study Fuel Cycle Study Bulk Controllability Of A Mixed-Oxide Fuelled CANDU-600 Using Frequency Response Analysis", AECL Internal Report CRNL-2617, 1984 January.
4. J.R. Lebenhaft and H.W. Hinds, "Bulk Controllability of Canflex-Fuelled CANDU-600 Using Frequency Response Analysis", AECL Internal Report CRNL-4218, 1988 February.

Table 1: Transfer function parameters and normalized gain at frequency of maximum coherence for all measured DNGS signals versus the average channel F ICFD signal as reference; and comparison to Effective Prompt Fractions from SDS2 trip test.

Signal	Frequency (Hz)	Gain	Phase (degrees)	Coherence	Normalized Gain at 0.25 Hz (%) (note 1)	1-σ statistical uncertainty in Gain	Effective Prompt Fraction (%) (note 2)
Lin_IC_F	0.281	0.777	-1.118	0.614	81.09	3.77	78.40
Lin_IC_J	0.244	0.718	-2.247	0.788	74.88	2.51	100.00
ICFD_1F	0.256	1.017	-0.748	0.975	106.13	1.19	102.75
ICFD_2F	0.256	1.025	-1.150	0.876	106.93	2.71	100.51
ICFD_3F	0.256	1.056	-1.495	0.955	110.19	1.67	102.31
ICFD_4F	0.244	0.971	1.020	0.938	101.38	1.80	101.32
ICFD_5F	0.256	0.940	-3.900	0.959	98.14	1.41	100.23
ICFD_6F	0.244	1.004	-1.845	0.940	104.78	1.84	102.46
ICFD_7F	0.256	0.837	-0.567	0.958	87.34	1.27	93.69
ICFD_8F	0.256	0.964	0.431	0.901	100.63	2.27	100.88
ICFD_9F	0.244	0.998	3.322	0.911	104.20	2.23	104.10
ICFD_10F	0.256	0.985	-0.990	0.798	102.84	3.36	101.18
ICFD_11F	0.281	1.004	2.494	0.893	104.79	2.46	104.10
ICFD_12F	0.256	1.197	3.700	0.699	124.94	5.06	97.38
ICFD_13F	0.256	1.070	1.970	0.970	111.62	1.38	100.59
ICFD_1J	0.256	1.060	-7.726	0.872	110.63	2.85	87.97
ICFD_2J	0.244	0.854	-1.178	0.927	89.12	1.72	88.65
ICFD_3J	0.256	0.836	0.372	0.584	87.28	4.24	89.67
ICFD_4J	0.244	0.849	-5.064	0.962	88.62	1.22	89.92
ICFD_5J	0.256	0.810	-2.188	0.968	84.54	1.07	88.99
ICFD_6J	0.269	0.829	-3.205	0.843	86.52	2.47	89.34
ICFD_7J	0.256	0.852	-3.908	0.858	88.96	2.42	91.23
ICFD_8J	0.256	0.759	-1.765	0.861	79.18	2.13	84.60
ICFD_9J	0.256	0.913	3.460	0.976	95.29	1.05	90.80
ICFD_10J	0.256	0.899	-0.566	0.976	93.83	1.04	89.96
ICFD_11J	0.256	0.906	8.020	0.957	94.60	1.39	89.48
ICFD_12J	0.256	0.831	-0.947	0.898	86.70	1.98	88.61
Avg_ICFD_J	0.256	0.861	-1.275	0.981	89.90	0.87	89.10

Notes:

1. All gains in this column are normalized to the design value prompt fraction or gain (89.9%) for the average channel J ICFD signal.
2. Ion Chamber J used as reference 100% prompt signal in trip analysis.

Table 2: Transfer function parameters and normalized gain at frequency of maximum coherence for selected PLGS signals versus the average channel D, E, and F ICFD signal as reference; and comparison to Effective Prompt Fractions from SDS1 trip test.

Signal	Frequency (Hz)	Gain	Phase (degrees)	Coherence	Gain (%)	1-σ statistical uncertainty (%)	Effective Prompt Fraction (%)
Avg PLGS A	0.171	1.038	5.802	0.983	103.83	1.4	93.9
Avg PLGS C	0.171	1.040	1.969	0.987	104.00	1.2	93.7
Avg PLGS D	0.171	1.012	0.041	0.998	101.24	0.5	99.4
Avg PLGS E	0.171	0.997	0.412	0.995	99.74	0.7	99.5
Avg PLGS F	0.171	0.989	-0.460	0.996	98.92	0.6	99.6
Avg PLGS G	0.171	0.940	0.796	0.986	93.98	1.1	95.5
Avg PLGS H	0.183	0.983	0.186	0.971	98.34	1.7	94.4
Avg PLGS J	0.171	0.945	-0.655	0.976	94.54	1.5	94.8
ICFD 1D	0.171	0.979	-0.421	0.988	97.89	1.1	99.3
ICFD 2D	0.183	1.090	2.915	0.943	109.04	2.6	99.2
ICFD 3D	0.171	1.026	-0.103	0.991	102.62	1.0	100.0
ICFD 4D	0.171	0.959	-2.295	0.988	95.89	1.0	100.0
ICFD 5D	0.171	0.947	-1.490	0.971	94.67	1.6	98.6
ICFD 6D	0.171	1.043	-4.985	0.993	104.35	0.9	101.1
ICFD 7D	0.171	1.007	1.306	0.884	100.68	3.5	100.0
ICFD 8D	0.171	1.009	4.388	0.962	100.94	2.0	98.5
ICFD 9D	0.171	1.032	1.871	0.977	103.16	1.6	99.4
ICFD 10D	0.171	1.002	0.322	0.977	100.17	1.5	98.2
ICFD 11D	0.171	1.033	-0.493	0.990	103.28	1.0	99.2
ICFD 12D	0.171	1.051	-0.110	0.986	105.09	1.3	99.6
ICFD 1J	0.183	0.965	0.489	0.979	96.51	1.4	96.8
ICFD 2J	0.171	0.975	1.939	0.939	97.54	2.4	91.7
ICFD 3J	0.171	0.980	-0.857	0.540	98.03	7.1	96.7
ICFD 4J	0.171	0.918	-2.118	0.986	91.77	1.1	93.1
ICFD 5J	0.171	0.863	0.534	0.602	86.27	5.8	96.1
ICFD 6J	0.171	0.913	-1.880	0.987	91.28	1.1	94.1
ICFD 7J	0.171	0.999	-1.585	0.986	99.92	1.2	94.1
ICFD 8J	0.171	0.960	-2.022	0.987	95.98	1.1	95.8

	Population average gain at 0.16 Hz (%)	Population σ for gain at 0.16 Hz	Population average EPf from trip(%).	Population 1-σ for trip EPf
Channel A,C,D,E,F ICs	96.9	5.3	99.5	0.9
Channel A ICFDs	104.6	5.4	93.9	1.1
Channel C ICFDs	104.7	5.4	93.7	1.0
Channel D ICFDs	101.5	3.9	99.4	0.8
Channel E ICFDs	99.9	3.7	99.5	1.0
Channel F ICFDs	99.4	3.5	99.6	0.9
Channel G ICFDs	94.9	5.2	95.5	1.3
Channel H ICFDs	98.0	7.7	94.4	2.1
Channel J ICFDs	94.7	4.2	94.8	1.7

Table 3: Prompt Fractions of representative signals from PLGS 2% power de-rate data and comparison to EPf from subsequent Reactor Trip Test (No LZC shadow factor)

Detector Signal	Pf (derate)	EPf (trip)
Linear IC average	**1.00**	**0.99**
Linear IC σ	*0.05*	*0.02*
ROP SIG-R1D	1.01	0.99
ROP SIG-R2D	0.89	0.99
ROP SIG-R3D	0.95	1.00
ROP SIG-R4D	0.99	1.00
ROP SIG-R5D	1.02	0.99
ROP SIG-R6D	0.93	1.01
ROP SIG-R7D	0.92	1.00
ROP SIG-R8D	0.89	0.99
ROP SIG-R9D	0.92	0.99
ROP SIG-R10D	0.97	0.98
ROP SIG-R11D	0.92	0.99
ROP SIG-R12D	0.99	1.00
Channel D average	**0.95**	**0.99**
Channel D σ	*0.04*	*0.01*
Channel E average.	**0.97**	**0.99**
Channel E σ	*0.03*	*0.01*
Channel F average	**0.98**	**1.00**
Channel F σ	*0.04*	*0.01*
Channel G average	**0.98**	**0.96**
Channel G σ	*0.04*	*0.01*
Channel H average	**0.96**	**0.94**
Channel H σ.	*0.06*	*0.02*
Channel J average	**0.95**	**0.95**
Channel J σ.	*0.07*	*0.02*

Table 4: Prompt Fractions for RRS ICFDs (Channels A & C) from PLGS 2% power de-rate data and comparison to EPfs from subsequent reactor trip test (with LZC shadow factors)

Detector	Reference LZC signal	LZC shadow factor	Pf (derate)	EPf (trip)
P1U VFD CH A	LZC_1	0.071	0.93	0.93
P2U VFD CH A	LZC_2	0.082	0.94	0.94
P3U VFD CH A	LZC_3	-0.037	0.81	0.94
P4U VFD CH A	LZC_4	0.066	0.95	0.92
P5U VFD CH A	LZC_5	0.086	0.92	0.96
P6U VFD CH A	LZC_6	0.053	0.97	0.94
P7U VFD CH A	LZC_7	0.139	0.89	0.93
P8U VFD CH A	LZC_8	0.173	0.91	0.93
P9U VFD CH A	LZC_9	0.185	0.99	0.95
P10U VFD CH A	LZC_10	0.062	0.92	0.93
P11U VFD CH A	LZC_11	0.068	1.01	0.94
P12U VFD CH A	LZC_12	0.065	0.96	0.96
P13U VFD CH A	LZC_13	0.136	0.99	0.93
P14U VFD CH A	LZC_14	0.155	0.95	0.95
Channel A average		**0.093**	**0.94**	**0.94**
Channel A σ		**0.047**	**0.04**	**0.01**
AVG_A	LZC_AVG	0.099	0.96	
P1U VFD CH C	LZC_1	0.097	0.97	0.93
P2U VFD CH C	LZC_2	0.119	0.97	0.93
P3U VFD CH C	LZC_3	0.011	0.91	0.94
P4U VFD CH C	LZC_4	0.063	0.96	0.93
P5U VFD CH C	LZC_5	0.084	0.92	0.95
P6U VFD CH C	LZC_6	0.047	0.95	0.93
P7U VFD CH C	LZC_7	0.144	0.92	0.94
P8U VFD CH C	LZC_8	0.151	0.90	0.93
P9U VFD CH C	LZC_9	0.161	0.97	0.94
P10U VFD CH C	LZC_10	0.043	0.94	0.92
P11U VFD CH C	LZC_11	0.041	0.96	0.94
P12U VFD CH C	LZC_12	0.071	0.93	0.96
P13U VFD CH C	LZC_13	0.116	0.97	0.93
P14U VFD CH C	LZC_14	0.133	0.96	0.94
Channel C average		**0.091**	**0.95**	**0.94**
Ch C σ		**0.046**	**0.02**	**0.01**
AVG_C	LZC_AVG	0.093	0.96	

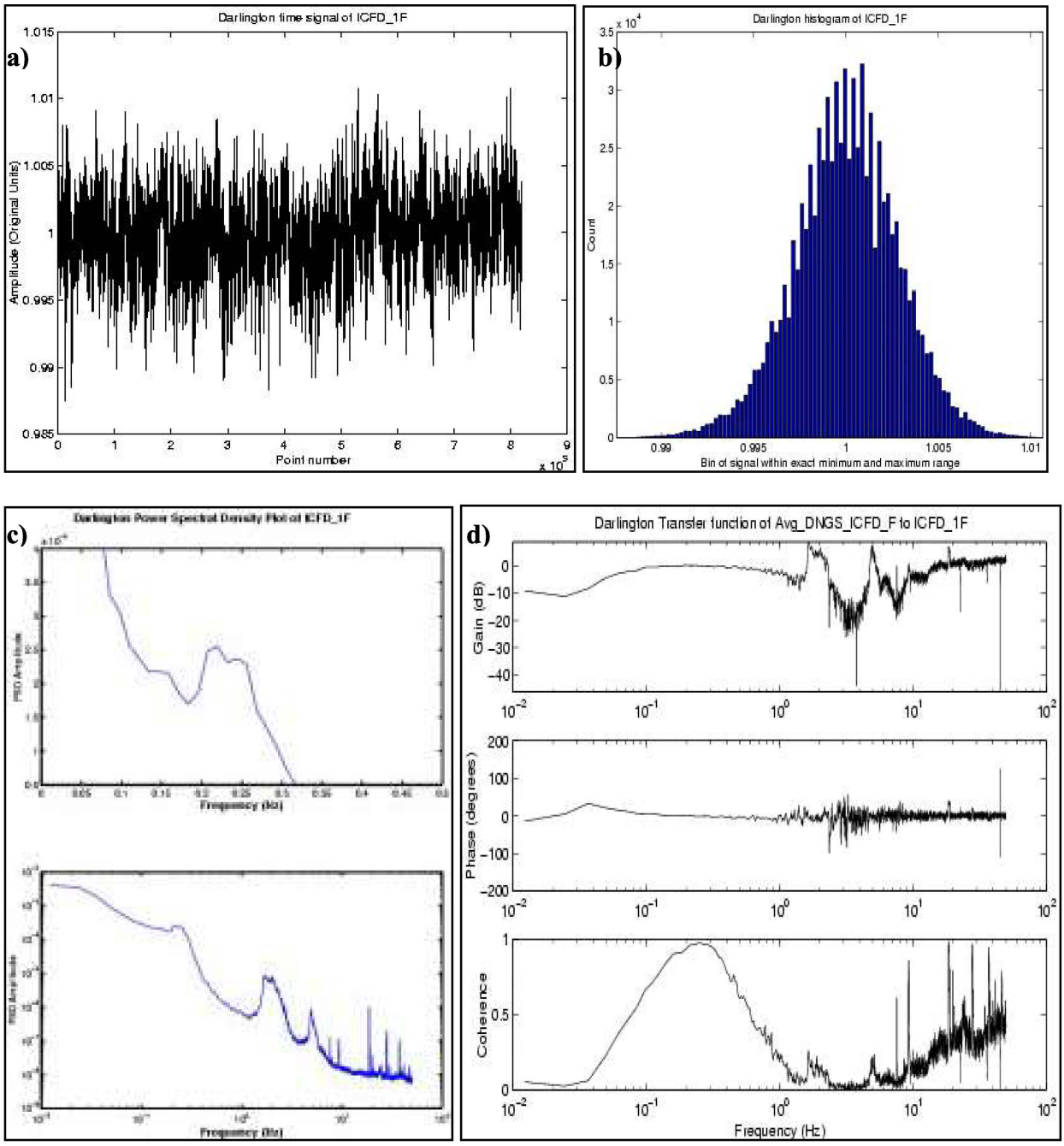

Figure 1: Plots of (a) normalized time-sequence data, (b) amplitude distribution histogram, (c) power spectral density, and (d) transfer function and coherence, for DNGS Unit 1 ICFD 1F ("Typical" Signal).

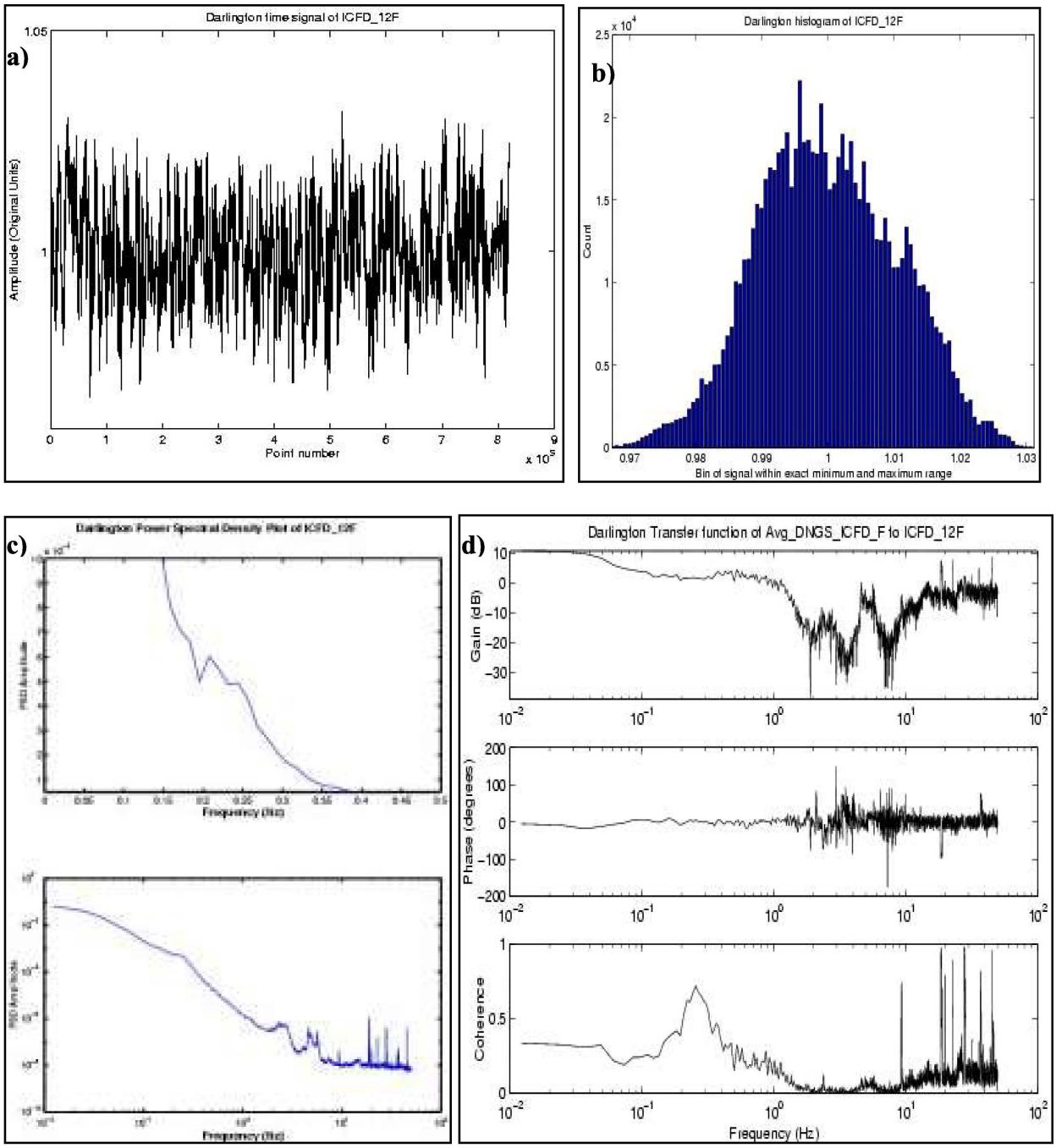

Figure 2: Plots of (a) normalized time-sequence data, (b) amplitude distribution histogram, (c) power spectral density, and (d) transfer function and coherence for DNGS Unit 1 ICFD 12F("Noisy" Signal)

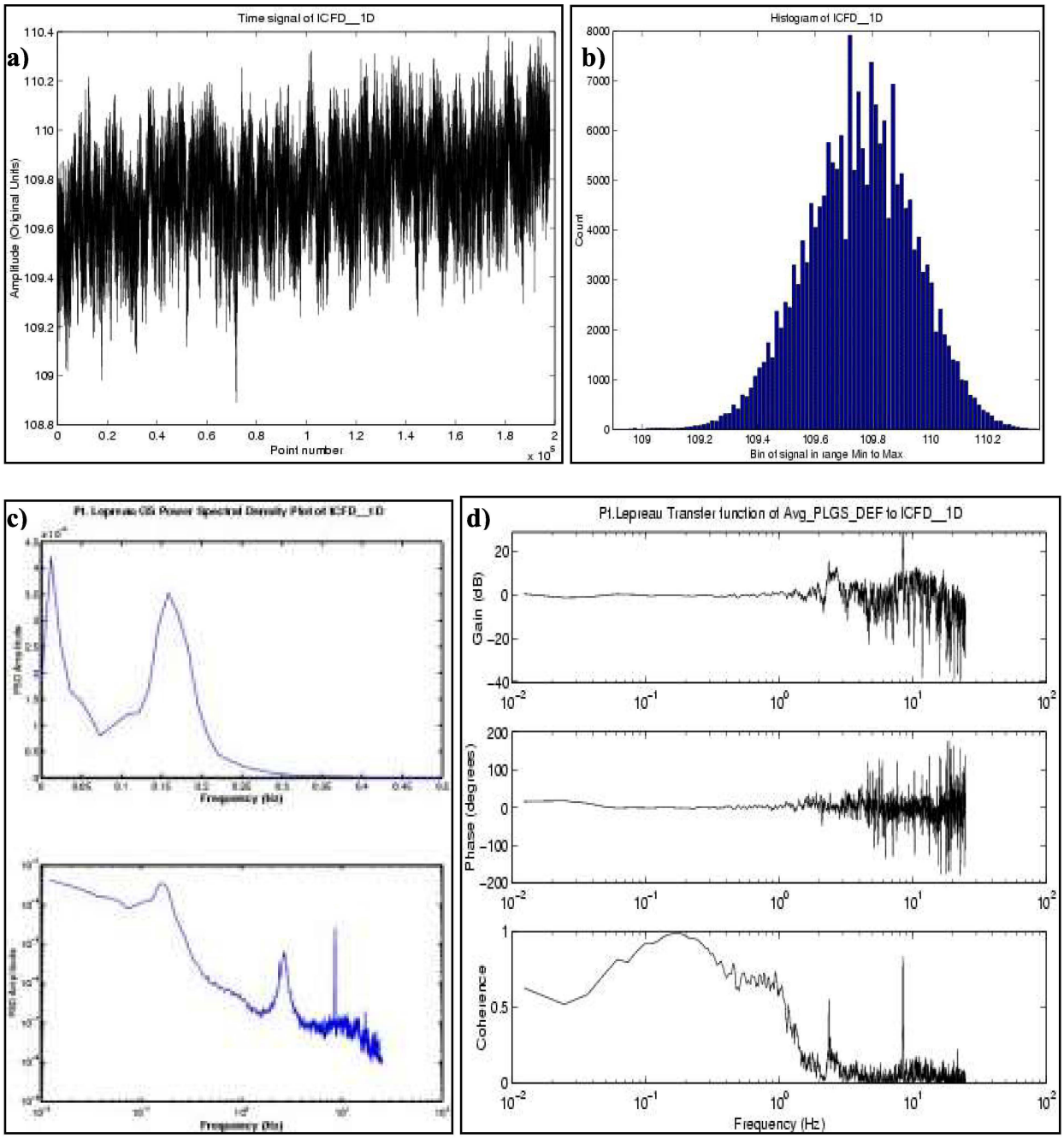

Figure 3: Plots of (a) raw time-sequence data, (b) amplitude distribution histogram, (c) power spectral density, and (d) transfer function and coherence for PLGS ICFD 1D ("Typical" Signal)

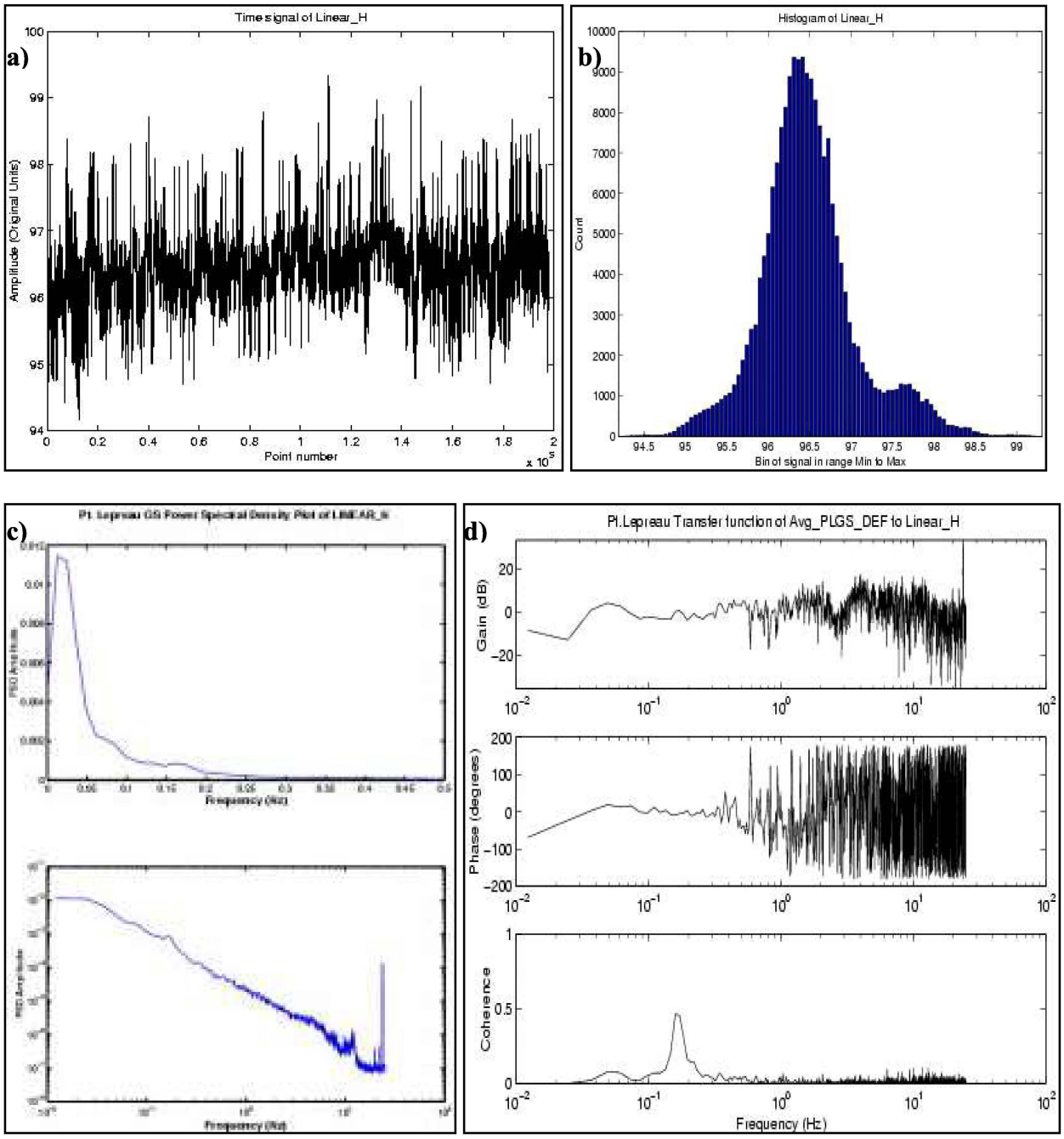

Figure 4: Plots of (a) raw time-sequence data, (b) amplitude distribution histogram, (c) power spectral density, and (d) transfer function and coherence for PLGS Linear IC Channel H ("Noisy" Signal)

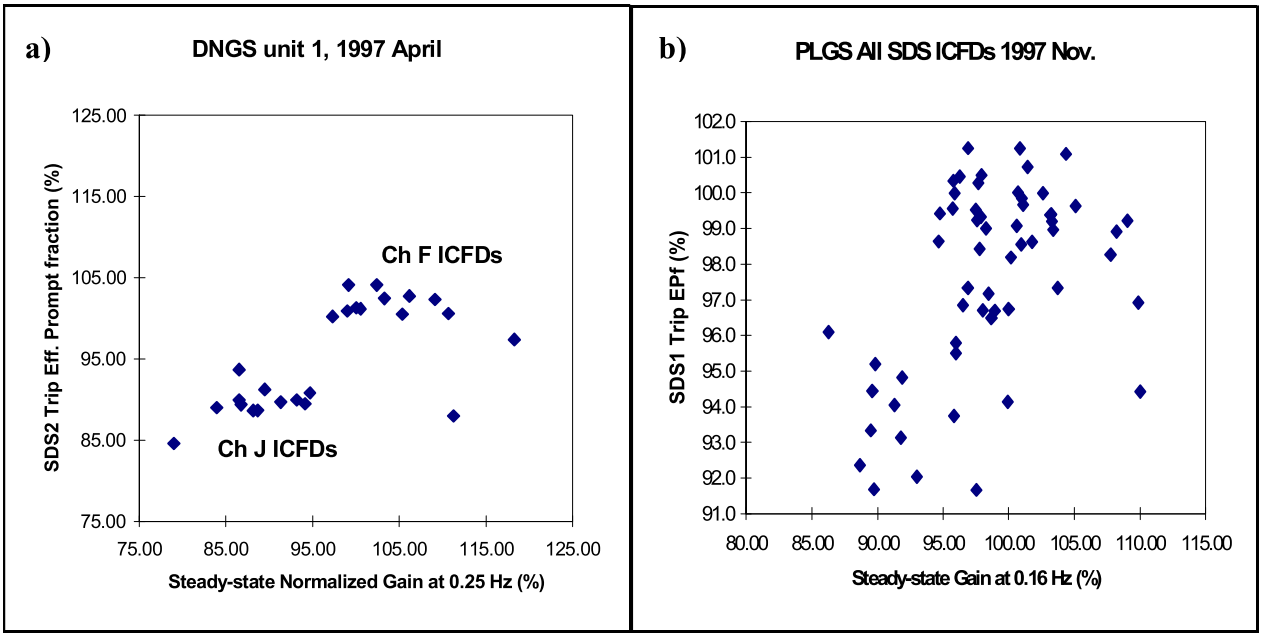

Figure 5: Comparison of Effective Prompt Fractions measured in trip test vs normalized High-frequency gain from steady-state data: (a) for DNGS Unit 1, and (b) for PLGS.

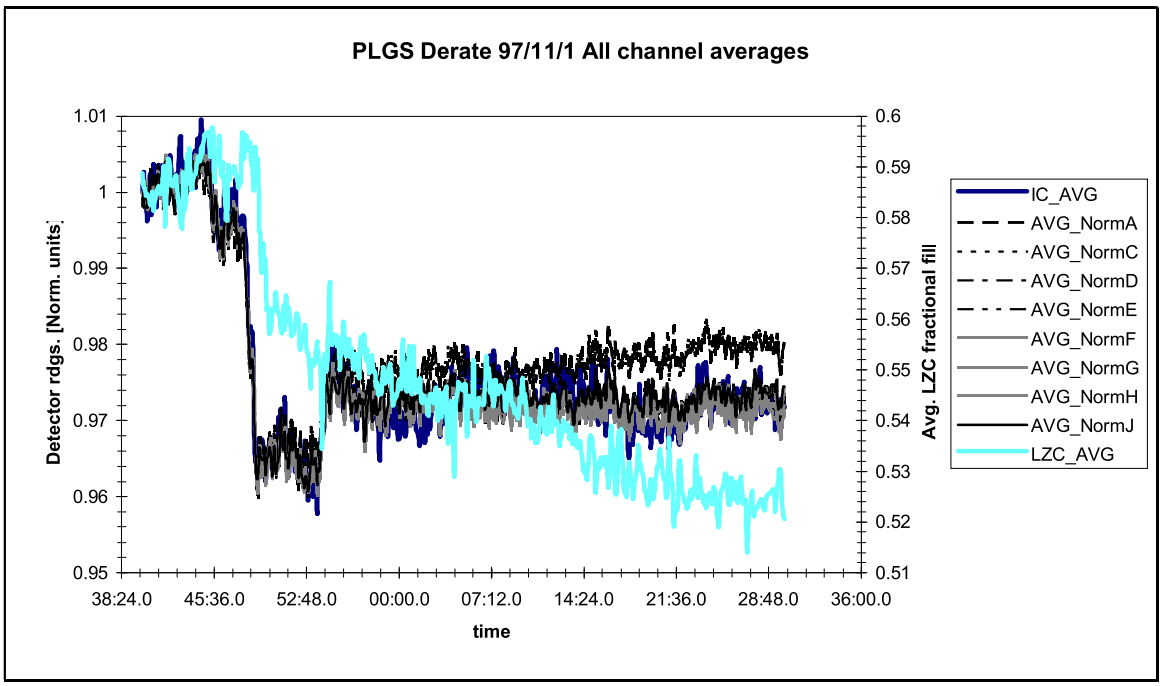

Figure 6: Core-Average Signals for PLGS Small Power De-Rate Maneuver

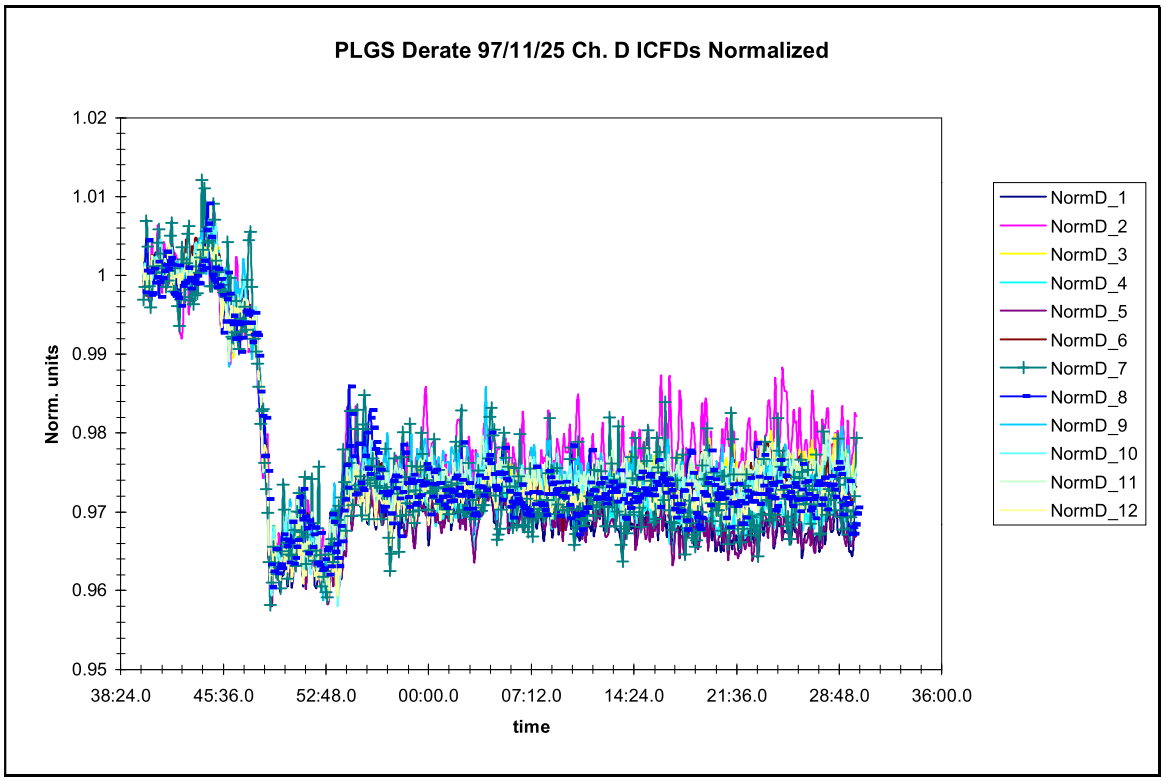

Figure 7: Normalized Signals from all Channel D ICFDs for PLGS Power De-Rate

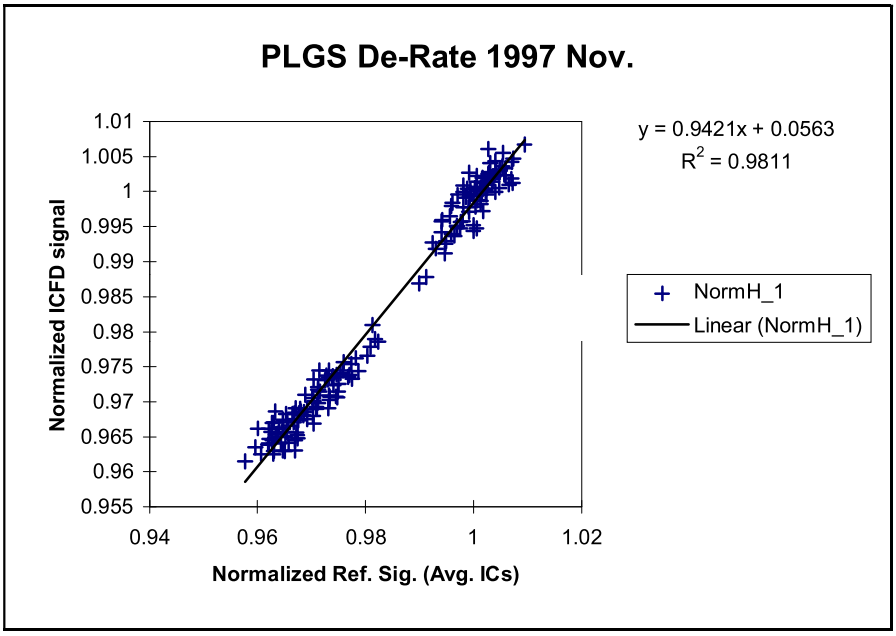

Figure 8: Scatter Plot of Measured ICFD Signal (ICFD_1H) vs Reference Signal During Small Power De-Rate

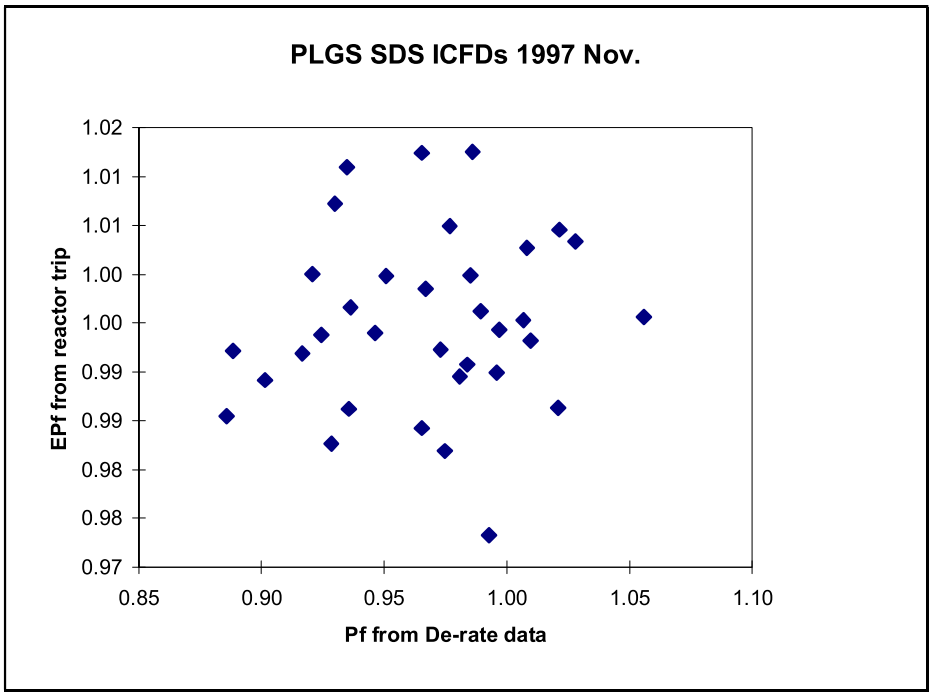

Figure 9: Trip EPf versus Pf from 2% power derate for all PLGS SDS ICFDs